Hydrogen oxidation on graphene-covered Pt(111) electrodes

Boterman, K.; Koper, M.T.M.

Electrochimica Acta 550 (2026) 148131

Contents lists available at ScienceDirect

Electrochimica Acta

journal homepage: www.journals.elsevier.com/electrochimica-acta

Hydrogen oxidation on graphene-covered Pt(111) electrodes

Katinka Boterman, Marc T.M. Koper *

Leiden Institute of Chemistry, Leiden University, 2300 RA Leiden, the Netherlands

ARTICLE INFO

Keywords:
Hydrogen oxidation
Pt(111)
Graphene
Electrocatalysis

ABSTRACT

Membrane-coated electrocatalysts offer a promising solution for current challenges in electrocatalysis, such as the susceptibility of the hydrogen oxidation reaction (HOR) to impurities. However, the understanding of how such coatings influence electrochemical processes remains limited. In this study, we present graphene-covered Pt (111) as a model system to investigate these effects. Graphene, known for its chemical stability and tunability, serves as a representative membrane, while Pt(111) is a well-known HOR catalyst that provides a useful comparison. The defect density in the graphene was systematically varied electrochemically and quantified using a proton-permeation resistance, measured with electrochemical impedance spectroscopy. We found that significant HOR activity is only obtained beyond a critical defect density. This suggests that molecular hydrogen permeation requires larger defect structures compared to atomic-scale defects that facilitate proton transport. Beyond this critical defect density the limitation of H_2 mass transport is also observed. We also show evidence that multi-layer graphene structures do not allow for effective HOR. Additionally, we observed a potential-dependent change in catalytic performance: cycling below 1.0 V led to a decrease in HOR current, while cycling to more positive potentials led to an increase. We attribute this behavior to potential-induced structural changes in the graphene layer. This study thereby highlights the importance of understanding the dynamic behavior of catalyst coatings in relation to their catalytic performance.

1. Introduction

Membrane-coated electrocatalysts are becoming an increasingly popular strategy in improving the performance and stability of electrocatalysts. In these systems, the active catalyst surface is covered with a thin, often nanometer-scale, overlayer that alters the surface properties or tunes the access of different electrolyte species to the active surface [1]. A particularly relevant reaction that may profit from a membrane coating is the hydrogen oxidation reaction (HOR) on platinum-group catalysts, since it is susceptible to poisoning by trace CO impurities in the H_2 feed gas [2,3]. Being able to control CO poisoning is expected to enhance catalyst activity and life-time [4].

Common strategies to increase CO-tolerance typically utilize alloys that either enhance CO oxidation through a bifunctional effect or weaken CO binding through an electronic effect [5,6]. However, recently, Tang et al. [7] used a RuO_2 shell on Ru, with the RuO_2 shell physically blocking CO from reaching Ru and adsorbing. This work demonstrated that a membrane-coated electrocatalyst could be a promising catalyst design strategy for CO-tolerant HOR.

Among various membrane materials, graphene, a single layer of carbon in a honeycomb lattice, has gained special attention. Graphene is chemically inert, mechanically robust, atomically thin, and can be synthesized on a relatively large scale with a high level of control via chemical vapor deposition (CVD) [8–12]. These properties make graphene an interesting candidate for membranes in electrochemical systems. In particular, graphene's well-defined atomic structure makes it an attractive model system for studying how reactions occur at membrane-coated electrocatalysts [13,14].

Graphene has already demonstrated beneficial membrane properties under electrochemical conditions. Initially, gas-phase studies showed that graphene protects Cu surfaces from oxidation [15,16]. Later, this effect was also shown for Cu and Ni under electrochemical conditions [14]. In these cases, graphene acts as a barrier, physically blocking oxygen from reaching the metal surface [14]. On a Pt(111) electrode, a well-studied surface in electrochemistry, graphene acts as a proton-selective membrane. Protons can reach the Pt(111) surface and adsorb, while electrolyte anions are completely blocked [17]. Electrochemically, this proton transport was quantified using electrochemical impedance spectroscopy by identifying the resistance to proton permeation ($R_{permeation}$) [18]. The magnitude of this resistance is directly

* Corresponding author.
E-mail address: m.koper@chem.leidenuniv.nl (M.T.M. Koper).

https://doi.org/10.1016/j.electacta.2026.148131
Received 13 November 2025; Received in revised form 28 December 2025; Accepted 4 January 2026
Available online 5 January 2026

related to the amount of defects in the graphene layer, suggesting that defects are the main proton transport channel under these conditions [18].

Interestingly, graphene-covered Pt(111) (Gr-Pt(111)) can also enhance the electrocatalytic hydrogen evolution reaction compared to bare Pt(111). DFT calculations predict that Gr–Pt(111) binds hydrogen slightly more weakly than Pt(111), which, according to Sabatier's principle, should enhance HER activity [19–21]. However, this enhancement is only observed when defects are present in the graphene layer, suggesting that the proton transport through pristine graphene is limiting the overall reaction. This kind of membrane permeation or "accessibility" limitation is a common concern in membrane-coated electrocatalysts [1].

In this work, we aim to expand our understanding of graphene-covered electrocatalysts by examining the performance of Gr–Pt(111) for the hydrogen oxidation reaction (HOR). This reaction, the reverse of HER, involves the oxidation of hydrogen molecules into protons in acidic media. Studying HOR on Gr-Pt(111) is compelling for several reasons. First, as mentioned earlier, HOR is especially sensitive to gas-phase impurities like CO, which graphene coatings may help mitigate. Second, since HER has already been shown to be enhanced by graphene, it is valuable to investigate whether similar behavior occurs for the reverse process. Lastly, HOR involves molecular hydrogen as the reactant, which is larger than protons and may display different permeation behavior through the graphene overlayer.

To explore these aspects, we grow graphene on Pt(111) using an established CVD method. The resulting Gr–Pt(111) electrodes are evaluated for HOR activity and stability using a rotating disk electrode (RDE) setup. This study will not yet consider the role of CO, as HOR on Gr-Pt(111) turns out to be sufficiently complex that it warrants a study on its own. We demonstrate that, similar to HER, the activity of HOR is closely linked to the presence of defects in the graphene layer. Additionally, we show that HOR performance is strongly affected by the potential-dependent stability of the graphene overlayer.

2. Methods

2.1. Electrolyte and glassware

All glassware was stored overnight in a 1g/L $KMnO_4$ solution acidified with H_2SO_4. The glassware was removed from $KMnO_4$ and immersed in a dilute H_2O_2/H_2SO_4 solution for at least 5 minutes, after which the glassware was rinsed and boiled in Milli-Q water five times. Electrolytes were prepared using H_2SO_4 (96%, Merck Suprapur) and Milli-Q water ($\geq$18.2 MΩ cm, TOC $<$ 5 ppb). The electrolytes were purged with Ar (5.0 purity, Linde) and H_2 (5.0 purity, Linde). C_2H_4 (3.0 purity, Linde) was used for the synthesis of graphene.

2.2. Electrode preparation

A Pt(111) single crystal (MaTeck, 6 mm diameter, 99.999%) was used as the working electrode. Before each experiment, the electrode was prepared based on the Clavilier method [22]. The crystal was flame annealed in two butane torches for 4 minutes and cooled in Ar/H_2 (80:30 ml min^{-1}) to clean the surface and remove previously grown graphene layers. The graphene layer was prepared using ambient pressure chemical vapor deposition (CVD) with induction heating according to the method of Fu et al. [17]. In this work, we preheat the crystal to ~1000°C in 200 ml min^{-1} pure H_2 for 5 minutes before dosing 2 ml min^{-1} C_2H_4 for 4 minutes. After these 4 minutes, the C_2H_4 bottle was closed, but the heat and H_2 stayed on for 1.5 minutes to allow for H_2 etching of the multilayers [23–25]. Subsequently, the heat was switched off and the crystal was cooled down for a minimum of 3 minutes in pure H_2 before transferring to the electrochemical cell.

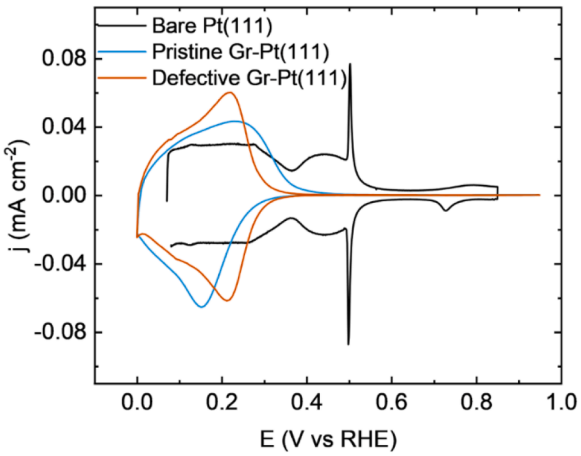

Fig. 1. CVs of bare Pt(111) and Gr-Pt(111), pristine and defective, measured at 50 mV/s in 0.1 M H_2SO_4.

2.3. Electrochemical methods

Electrochemical experiments were performed in a three-electrode system using a Biologic SP-300 potentiostat. Pt(111) (with graphene) served as the working electrode, a Pt wire (99.99%) was used as the counter electrode, and a reversible hydrogen electrode (RHE, HydroFlex, Gaskatel) was employed as the reference. A 10 μF shunt capacitor was connected between the reference and an additional Pt wire (99.99%) to reduce high-frequency noise. Electrode rotation was controlled using an MSR rotator (Pine Research Instrumentation) with a custom tip to attach the single crystal disk to the shaft.

The electrolyte was purged with Ar for at least 10 minutes prior to electrochemical experiments to remove oxygen. The working electrode makes contact with the solution in a hanging meniscus configuration under potential control of 0.05 V vs RHE. Cyclic voltammetry between 0.05 and 0.85 V on bare Pt and 0 to 0.95 V on Gr-Pt(111) was used as electrochemical characterization. Electrochemical impedance spectroscopy (EIS) was used to measure the hydrogen permeation resistance at 0.15 V vs RHE at frequencies between 10 kHz and 0.1 Hz and 5 mV amplitude [18].

To generate defects in the graphene layers, the potential was cycled between -0.1 and 1.3 V at 500 mV/s, where the positive potential limit and the number of cycles depended on the effect, i.e., defect density, to be achieved.

Before all hydrogen oxidation reaction experiments, the cell was purged with Ar for at least 10 minutes to remove oxygen and then for at least 10 minutes with H_2 to saturate the solution. During measurements, H_2 is continuously purged over the solution in the headspace of the electrochemical cell. At the beginning of each HOR measurement, the ohmic resistance was determined by EIS, which was 85% compensated in the Biologic software. Ten Gr-Pt(111) samples were prepared for the HOR activity study. Five samples in total were prepared to study the potential dependent stability of Gr-Pt(111).

2.4. Graphene characterization

Raman spectra of Gr-Pt(111) were recorded on a WITEC alpha 300 R Confocal Raman Imaging system with a 457 nm laser wavelength, with a maximum 5 mW laser power. The graphene layer was imaged using a Thermo Scientific Apreo scanning electron microscope operating at 2 keV and 0.1 nA beam current.

Gold deposition is performed by cycling between 0.0 and 0.6 V in a solution containing 0.1 M H_2SO_4 + 5 μM $AuHCl_4$ (99.995% trace metal basis, Sigma-Aldrich) [18,26,27].

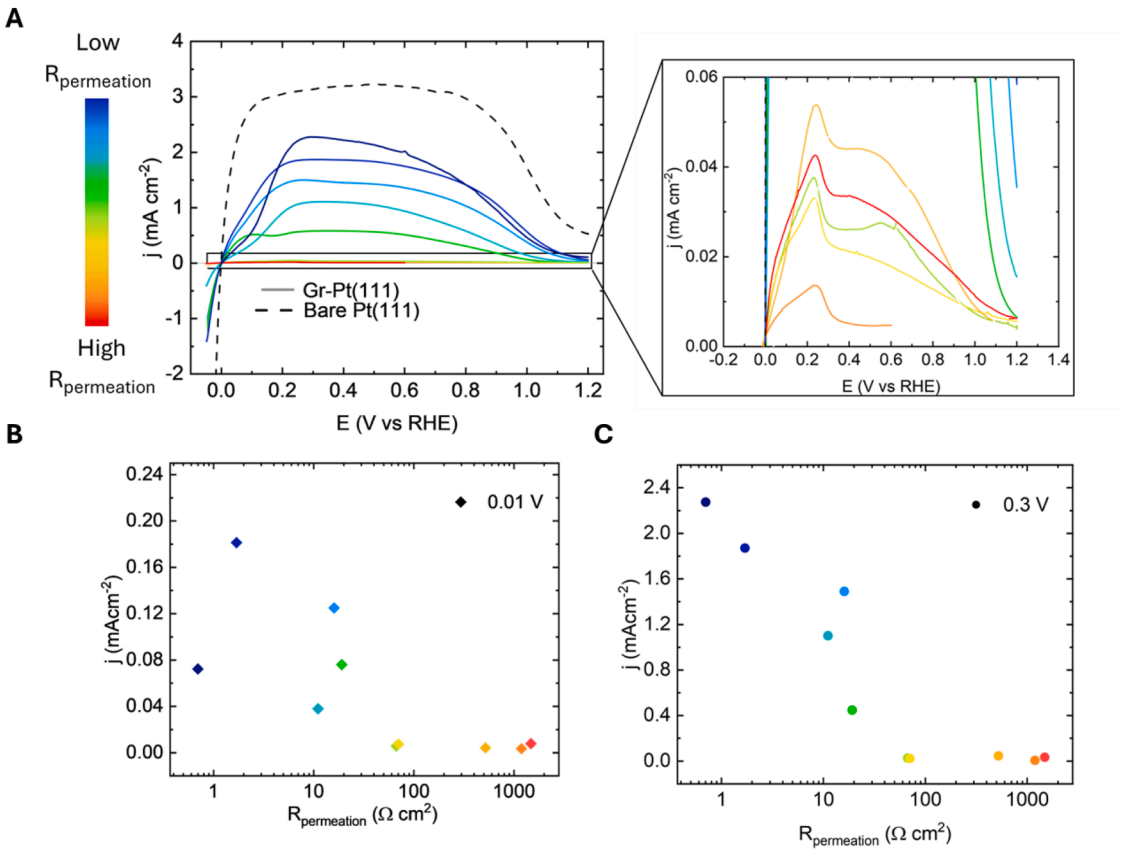

Fig. 2. (A) Forward scan of CVs for HOR, recorded between –0.05 and 1.2 V vs RHE at 10 mV/s and 1600 RPM in H_2 saturated 0.1 M H_2SO_4. Curves compare bare Pt (111) (dotted line) with Gr–Pt(111) at different defect densities. Current density at (B) 0.01 V and (C) 0.3 V vs. $R_{permeation}$.

3. Results and discussion

3.1. The Gr-Pt(111) electrode

The quality of both the bare Pt(111) surface and the graphene-covered surface was assessed using cyclic voltammetry (CV) in 0.1 M H_2SO_4. As shown in Fig. 1, the CV of bare Pt(111) shows the characteristic features of the hydrogen under-potential deposition (H_{upd}) between 0 and 0.35 V vs RHE and the "butterfly" adsorption feature of sulfate between 0.35 and 0.55 V. The CV of Gr-Pt(111) is different depending on the state of the graphene layer. The pristine Gr-Pt(111) exhibits an asymmetric H_{upd} region and an HER onset below 0 V vs. RHE, both of which indicate high resistance to proton permeation ($R_{permeation}$). In contrast, the defective Gr-Pt(111), prepared using oxidative-reductive cycling, shows a more symmetrical H_{upd} feature consistent with a lower $R_{permeation}$. [18,28]. Notably, both Gr-Pt(111) samples show no sign of the characteristic sulfate adsorption features between 0.35-0.55 V. This means that the graphene layer specifically inhibits anions (in this case sulfate) from adsorbing on the Pt(111) surface, while hydrogen adsorption is still possible. This shows that the graphene layer acts as a selective membrane (although there is evidence that anions interact with the defects [18,28]). The reproducibility of the CV for different CVD growths can be found in SI Fig. 1, together with a representative Nyquist plot and the equivalent circuit used to obtain $R_{permeation}$. To further characterize the surface, SEM, Raman spectroscopy, and Au deposition were used, shown in SI Figs. 2-4. These techniques consistently confirm that the surface is covered with a layer of graphene with relatively low defect density. Additionally, multilayer spots are observed, which account for approximately 20% of the surface.

3.2. HOR activity and graphene defects

The forward scans of HOR CVs for Gr-Pt(111) with different defect densities, compared to bare Pt(111), are shown in Fig. 2A. Before each HOR experiment, defects were created using potential cycling, which lowers $R_{permeation}$. The number of cycles was varied to obtain a range of $R_{permeation}$ values. The CV of bare Pt(111) exhibits the well-known behavior, where the current initially increases strongly, as Pt is a good catalyst for HOR. Around 0.1 V, the current reaches a plateau, from which potential the current is potential independent and fully limited by mass transport [29]. This diffusion-limited current can be predicted using the Levich equation for different rotation rates [29,30]. From Fig. 2A, it is clear that the HOR activity strongly varies with the graphene defect density, as expressed in $R_{permeation}$. However, none of the measured samples reach the predicted diffusion-limited current for HOR, while a plateau is still present. This indicates that mass transport limitations alone do not fully account for the observed behavior. The rotation-rate dependent mass transport limitations of this system will be described in more detail in the next section. The fact that this plateau is not perfectly flat, like on bare Pt(111), is hypothesized to originate from the accumulation of anionic species around defects, since we also observe the steep current density decrease around 0.9 V on both bare Pt (111) and Gr-Pt(111). On Pt, this steep decay is explained by the adsorption of oxide species on the Pt surface [29,31]. We expect the origin of this decrease on Gr-Pt(111) to be similar in nature, where an anionic species is blocking the surface at or near defect sites, which lowers the activity.

To further investigate the dependence of HOR activity on defect density, we plot the HOR activity at 0.3 V, in the mass transport limited regime, and 0.01 V, before mass transport limitations, as a function of $R_{permeation}$ in Fig. 2B and C. At both potentials, two regimes appear to

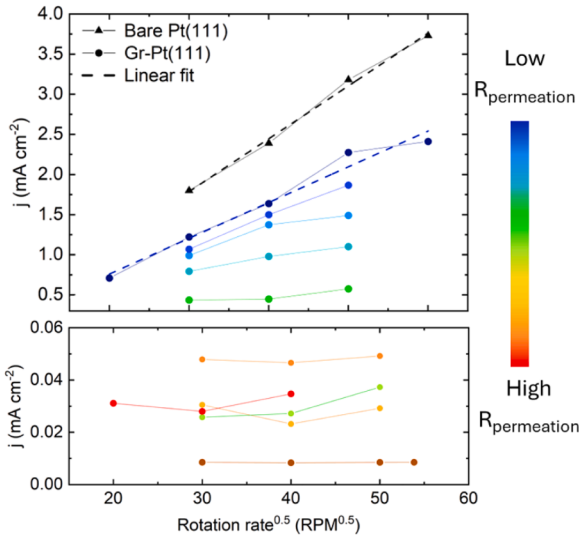

Fig. 3. Dependence of current density at 0.3 V on rotation rate for bare Pt(111) compared to Gr–Pt(111) surfaces with increasing defect density.

exist. In the first regime, samples with high values of $R_{permeation}$ show negligible HOR activity that is independent of $R_{permeation}$. This suggests that the graphene layer blocks hydrogen from reaching the Pt surface to perform the reaction. Additionally, introducing more defects does not facilitate HOR in the same way it does for proton permeation. As $R_{permeation}$ lowers, protons experience less resistance to permeate and adsorb on Pt, but the results in Fig. 2B and C indicate that this is not necessarily true for the hydrogen molecule.

Below an (apparent) threshold value of $R_{permeation}$ we enter a second regime where the HOR activity rapidly increases and strongly correlates with $R_{permeation}$. This suggests the existence of a critical defect density for HOR to be significant. This behavior is observed at both potentials, meaning there is a similar effect on the kinetically- and diffusion-limited current. The trend is less pronounced at 0.01 V, which can be attributed to a greater variability in current profiles across samples at low overpotentials.

It is important to note that $R_{permeation}$ reflects proton permeation resistance rather than molecular H_2 permeation resistance. The size difference between protons and H_2 molecules may therefore explain the observed relationship between the HOR current density and $R_{permeation}$. Proton permeation through graphene has been hypothesized to occur via atomic-scale point defects that are either inherently present or generated in the lattice [17,28]. In pristine graphene, the dominant defect sites, and thus the primary permeation pathways, are grain boundaries between graphene domains [18]. The results presented in Fig. 2 indicate that these grain boundaries are sufficient for proton transport but insufficient to enable significant H_2 permeation. Due to their larger size, H_2 molecules are expected to require either a higher local defect density or larger defect structures for permeation [32,33].

Oxidative–reductive cycling introduces additional point defects into the graphene layer [18]. Fig. 2 suggests that beyond a certain degree of oxidative–reductive cycling, H_2 permeation becomes sufficient, consistent with the formation of defect structures capable of accommodating permeation of molecular hydrogen. We hypothesize that above a critical defect density, reflected by a sufficiently low $R_{permeation}$, these point defects created larger openings or undergo chemical modification (e.g., incorporation of oxygen functional groups, see section Potential dependent stability), thereby altering their atomistic structure and enabling H_2 permeation. However, resolving the precise atomic nature of graphene defects at varying defect densities under electrochemical conditions requires specialized characterization techniques. Apparently, such defect structures only appear beyond a critical defect density, leading to the two distinct regimes observed in Fig. 2.

3.3. Rotation rate dependence on HOR activity

To further investigate the apparent diffusion limitation of the HOR current and to make a comparison with the uncovered surface, we studied the effect of rotation rate. As discussed, HOR on bare Pt(111) reaches a diffusion-limited current, which can be described by Levich equation:

$$j_L = 0.62nFD^{\frac{2}{3}}\nu^{-\frac{1}{6}}\omega^{\frac{1}{2}}c_0$$

with n being the number of electrons transferred ($n = 2$ for HOR), F the Faraday constant, D the diffusivity of hydrogen, ν the kinematic viscosity of the electrolyte, ω the rotation rate of the electrode, and c_0 the hydrogen concentration [30]. Here, the current scales with the square root of the rotation rate, with a theoretical slope of $6.54*10^{-2}$ (mA cm^{-2})*$RPM^{-1/2}$ [29,30]. In our experiments with bare Pt(111) shown in Fig. 3, a slope of $6.58*10^{-2}$ (mA cm^{-2})*$RPM^{-1/2}$ can be extracted, in agreement with theory.

The influence of rotation rate on the current in the (apparent) plateau region was also investigated for Gr-Pt(111), as shown in Fig. 3. For samples with low current densities, the measured current is largely independent of rotation rate, further indicating that permeation through the graphene layer, rather than solution diffusion, is the primary limiting factor. However, as the defect density increases, and we enter the second regime described in the section before, the current becomes increasingly dependent on the rotation rate. The linear dependence of the current density on the square root of the rotation rate suggests mass-transport control. The slope with the strongest dependence is $4.45*10^{-2}$ (mAcm^{-2})*$RPM^{-1/2}$, which is 32% lower than the theoretical Levich slope. The magnitude of the current density measured for Gr-Pt(111) compared to bare Pt(111) is between 28 and 35% lower for the different rotation rates. The fact that the scaling of the slope and magnitude of the current density are similar confirms the idea that in this regime, the current is mass-transport limited.

This deviation from bare Pt(111) can possibly be explained by an overestimation of the surface area used to normalize current to current density. The current was normalized by the geometric surface area of the electrode, which, for the atomically flat Pt(111) is a reasonable assumption of the active surface area. Also, on Gr-Pt(111), the charge of the H_{upd} reaches a full monolayer of hydrogen and does not change significantly between samples with different defect density [17]. However, as discussed before, this apparent lower active surface area can be caused by the limited permeation of the molecular hydrogen molecules, meaning that the surface area active for HOR is specifically different from that active for H_{upd}.

A possible origin of these blocked surface sites is the presence of multilayers of graphene. As can be seen in the SEM images in SI Fig. 3, there are spots of multilayer graphene. These spots make up around 20% of the total surface, fluctuating slightly between samples. We used Au deposition, a technique where Au selectively deposits on graphene defect sites [18,26,27], to visualize the defect formation on our samples. SI Fig. 4.2 clearly shows that the number of Au particles on multilayer sections is less than on the single layer sections, even after significant reduction of $R_{permeation}$. We therefore hypothesize that the multilayer sections of the graphene covered surface are the cause of the reduced surface area deduced from Fig. 3.

To summarize our hypothesis of how H_2 permeation and H_2 mass transport control the HOR activity of Gr-Pt(111), we combine the observations of Figs. 2 and 3. In the low current regime, the defect density (or size and structure of defects) is insufficient to facilitate H_2 permeation for significant HOR activity, and thus the current is entirely limited by slow H_2 permeation. As a result, the current is independent of the proton permeation resistance $R_{permeation}$ and the electrode rotation rate.

As the defect density decreases below an apparent critical defect density, the limitation of H_2 permeation is lowered to allow significant HOR activity. In this regime, further increasing defect density increases

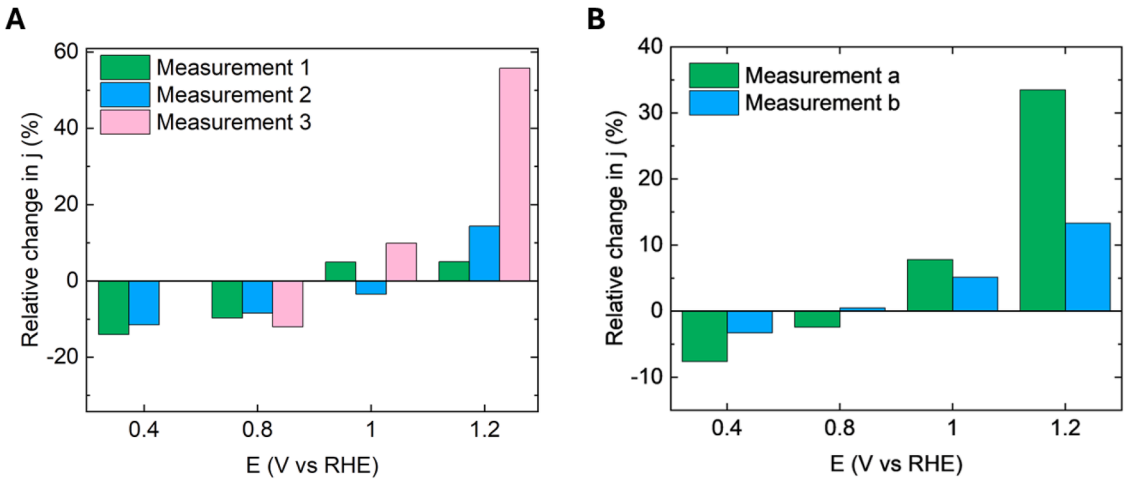

Fig. 4. (A) Relative change in current density at 0.4 V (in the forward scan) after six cyclic voltammetry (CV) cycles between 0 V and the upper potential limit indicated on the x-axis. (B) Relative change in current density at 0.4 V (in the forward scan) in CVs recorded before and after a 5-minute potential hold at the indicated potential on the x-axis. All measurements represent independent experimental repeats and were performed at 1600 RPM in H_2-saturated 0.1 M H_2SO_4. Panel (A) was recorded at a scan rate of 20 mV/s, and panel (C) at 50 mV/s.

the H_2 permeation and therefore, enhances HOR activity. As HOR becomes faster, the mass transport limitation of H_2 start to form a significant limitation to the activity. However, the multilayer sections of the surface remain largely impermeable to hydrogen molecules, which leads to an effectively lower active surface area, which is reflected in a deviation of the total mass transport limited current and the slope of the Levich plot.

3.4. Potential dependent stability

Following the observation that Gr–Pt(111) exhibits structure-dependent activity for the hydrogen oxidation reaction (HOR), we investigated how this activity evolves as a function of time and electrode potential. To this end, the upper potential limit of the cyclic voltammetry (CV) scan was varied. In each experiment in Fig. 4A, the CV was cycled between 0 V and a defined upper limit for six times, and the current at 0.4 V in the next positive-going scan was compared to the current in the first scan. When the upper limit remained below 1.0 V, the HOR current progressively decreased with each cycle. Interestingly, this trend reversed around 1.0 V, with cycling to 1.2 V leading to an increased activity. In a similar experiment, applying a potential for 5 minutes has the same effect on the CV current measured at 0.4 V in the following positive-going scan, as shown in Fig. 4B. Both observations indicate a pronounced potential dependence of the structure of the graphene on Pt(111) [33]. Having previously established that graphene defects are the main pathway for transporting reactants and products, leading to enhanced HOR activity, we hypothesize that a loss of activity is related to a lowering of the number of defect sites, or otherwise a change in the defect structure leading to lower activity. Potential causes include the accumulation of blocking species at the defects or structural changes that reduce access to the underlying Pt surface.

The only electrolyte species present are water, protons, and sulfate/bisulfate ions. Because the solution is already strongly acidic, the effect of protons generated during HOR is expected to be negligible. An effect of anions blocking the surface is expected to increase at higher potentials since anions will be more attracted to a more positive surface. However, our experiments show the opposite effect, with more positive potentials eventually showing an increase in activity. Therefore, we also exclude the blocking of anions as the main explanation for this effect.

Another plausible explanation is a potential-dependent structural transformation of graphene itself. Considering that our approach to create defects in the graphene layer involves cycling to these positive potentials, we assume that oxidation of defect sites or carbon atoms

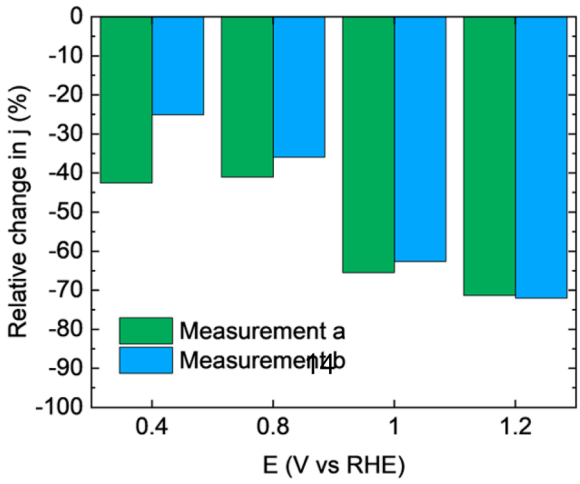

Fig. 5. Relative change in current density over a 5-minute chronoamperometric (CA) potential hold at the corresponding potential shown on the x-axis.

occurs [32,33]. While the full oxidation of carbon to CO_2 (or CO) is unlikely to be reversible, there is evidence that graphene can form oxygen functional groups in the lattice at oxidative potentials [33]. These functional groups, having similar characteristics to graphene oxide, could then be electrochemically reduced [33,34]. It is likely that sites like these have a different hydrogen permeability compared to a pristine lattice [35]. Using Au deposition, Arulmozhi et al. [18] showed that oxidative reductive cycling created more point defects in the graphene in addition to existing grain boundaries. In contrast, at lower potentials, graphene may slowly "heal" or restructure in a way that inhibits hydrogen permeation pathways, diminishing activity. Considering the observed changes are strongly potential dependent and taking into account the suggestion of reversible oxidation in literature, we hypothesize a role of oxidation and reduction of parts of the graphene lattice, however the exact mechanism at the atomic level cannot be resolved through electrochemical techniques alone. Therefore, extensive material characterization would be necessary to elucidate the possible role of the graphene structure or electrolyte effects in the observed phenomenon.

Although the CVs recorded before and after the potential hold show a potential-dependent trend, as discussed above, the current during the 5-

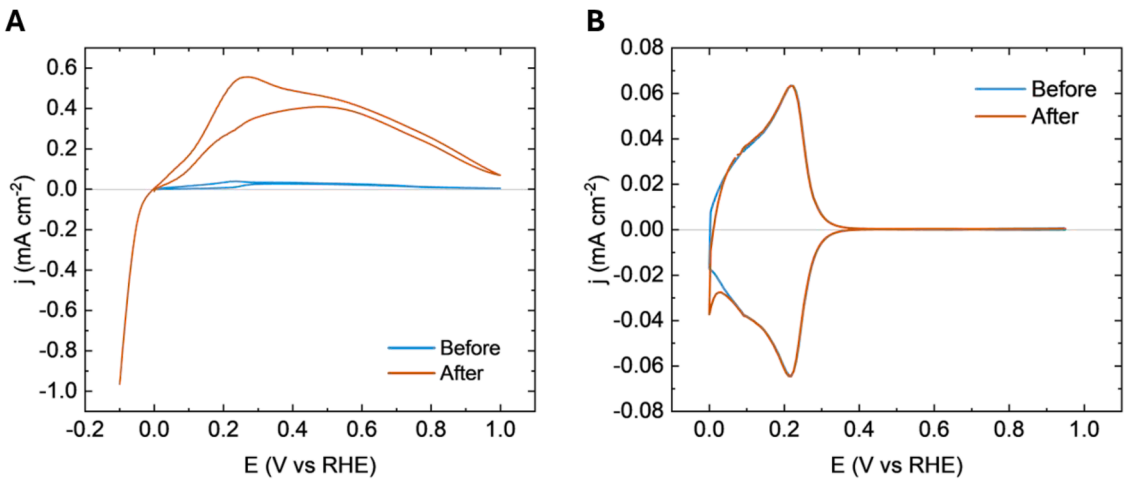

Fig. 6. (A) CVs of HOR before and after performing HER for 10 seconds at -0.1 V. Measured at 1600 RPM, 10 mV/s in H_2 sat. 0.1 m H_2SO_4.(B) CVs of Gr-Pt(111) before and after the experiment performed in panel A. at 0 RPM, 50 mV/s in Ar sat. 0.1 M H_2SO_4.

minute hold itself consistently decreases at all potentials (Fig. 5). This seems contradictory, considering that cycling to and holding the potential at 1.0 and 1.2 V leads to an increased activity measured at 0.4 V. This contrast suggests that the effect of potential during CV cycling differs from a time effect during potential holding.

One possible explanation for why, at high positive potentials, the current does not increase over time is the accumulation of species, such as anions or oxides, at the surface. This could lead to a poisoning effect that suppresses the current, even as the surface does undergo defect formation or restructuring. Even though the graphene layer prevents the direct adsorption of anionic species, it has been shown that the presence of anions changes the hydrogen adsorption/desorption kinetics [18]. This suggests that anions can block permeation through the defects by being present (or adsorbed) close to or within defects sites on the graphene surface. When the potential is subsequently cycled back toward 0 V, these accumulated species may be desorbed or displaced, effectively "cleaning" the surface. As a result, when the current is extracted at 0.4 V, the previously formed or restructured defect sites are now more accessible, potentially explaining the observed increase in HOR activity.

Alternatively, it is possible that the formation or restructuring of defect sites requires both oxidative and reductive conditions to change into the permeable form needed for the reaction. However, these mechanistic hypotheses cannot be confirmed solely through electrochemical data. Further investigation using complementary material characterization techniques would be needed to support this explanation.

We also investigated the effect of changing the negative potential limit. The results are shown in Fig. 6. Below 0 V, the hydrogen evolution reaction (HER) takes place, producing H_2 at the surface. Hydrogen bubbles can delaminate graphene from its metal substrate [36,37]. It is therefore expected that, without additional protection, graphene will be damaged by the formation of these bubbles [28]. Fig. 6A shows a strong increase in HOR current after performing HER. Additionally, Fig. 6B shows how the blank CV has changed, with the HER onset having shifted significantly, indicating that the graphene is more defective [18,28]. However, no features in the anion adsorption region have appeared, meaning that no delamination of larger pieces of the graphene layer took place.

4. Conclusions

In this work, we investigated both the activity and stability of the hydrogen oxidation reaction on graphene-covered Pt(111) to elucidate the role of the graphene layer as a catalyst coating. Our results demonstrate that the HOR activity on Gr–Pt(111) is strongly dependent on the defect density of the graphene layer. These defects serve as permeation pathways for H_2, enabling access to the underlying Pt surface. By correlating the measured proton permeation resistance $R_{permeation}$ with HOR current densities, we identified two distinct regimes.

At low defect density (high $R_{permeation}$), the current is limited by the permeation of H_2 molecules through the graphene layer. The atomic-scale defects that facilitate proton transport are insufficient for molecular H_2 permeation. As the defect density increases ($R_{permeation}$ decreases), a second regime emerges where HOR activity sharply increases and the current becomes mass-transport limited. The nonlinear dependence of H_2 permeation on defect density suggests that not only the defect density changes, but also the permeation ability (e.g. size) of the individual defects.

We further show that HOR activity is strongly influenced by the applied potential. Cycling the potential below 1.0 V reduces activity, while cycling potentials above 1.0 V increases activity, likely due to dynamic potential-dependent opening of the graphene layer. During prolonged potential holds, the current gradually decreases, which we attribute to accumulation of anions or oxide species near defects. Additionally, performing HER prior to HOR enhances activity, further suggesting that graphene damage increases H_2 permeation.

Overall, our findings highlight that graphene coatings affect catalytic performance by changing reactant permeation and active site accessibility, while also exhibiting potential-dependent changes in stability over time.

Declaration of competing interest

The authors declare that they have no known competing financial interests or personal relationships that could have appeared to influence the work reported in this paper.

Acknowledgments

This project received funding from project 20354 “Membrane-coated selective electrocatalyst for hydrogen production, purification, and compression” from the Open Technology Programme of the Dutch Research Council, with financial support from HyET Hydrogen, HyET E-Trol, and VEECO.

Supplementary materials

Supplementary material associated with this article can be found, in the online version, at doi:10.1016/j.electacta.2026.148131.

References

[1] D.V. Esposito, Membrane-coated electrocatalysts - An alternative approach to achieving stable and tunable electrocatalysis, ACS Catal. 8 (2018) 457–465, https://doi.org/10.1021/acscatal.7b03374.

[2] S.J. Lee, S. Mukerjee, E.A. Ticianelli, J. McBreen, Electrocatalysis of CO tolerance in hydrogen oxidation reaction in PEM fuel cells, Electrochim. Acta 44 (1999) 3283–3293, https://doi.org/10.1016/S0013-4686(99)00052-3.

[3] V.F. Valdés-López, T. Mason, P.R. Shearing, D.J.L. Brett, Carbon monoxide poisoning and mitigation strategies for polymer electrolyte membrane fuel cells – A review, Prog. Energy Combust. Sci. 79 (2020) 100842, https://doi.org/10.1016/j.pecs.2020.100842.

[4] J.-T. Ren, L. Chen, H.-Y. Wang, Y. Feng, Z.-Y. Yuan, Hydrogen oxidation electrocatalysts for anion-exchange membrane fuel cells: activity descriptors, stability regulation, and perspectives, Energy Environ. Sci. 17 (2024) 3960–4009, https://doi.org/10.1039/D3EE04251K.

[5] A. Baz, A. Holewinski, Understanding the interplay of bifunctional and electronic effects: microkinetic modeling of the CO electro-oxidation reaction, J. Catal. 384 (2020) 1–13, https://doi.org/10.1016/j.jcat.2020.02.003.

[6] J. Byeon, S. Kim, S. Lee, J.H. Jang, S.K. Kim, J. Lee, CO-tolerant electrocatalysts for hydrogen fuel cells: fundamental study-based design and real-life applications, Chem. Eng. J. 493 (2024) 152626, https://doi.org/10.1016/j.cej.2024.152626.

[7] T. Wang, L.Y. Li, L.N. Chen, T. Sheng, L. Chen, Y.C. Wang, P. Zhang, Y.H. Hong, J. Ye, W.F. Lin, Q. Zhang, P. Zhang, G. Fu, N. Tian, S.G. Sun, Z.Y. Zhou, High CO-tolerant Ru-based catalysts by constructing an oxide blocking layer, J. Am. Chem. Soc. 144 (2022) 9292–9301, https://doi.org/10.1021/jacs.2c00602.

[8] X. Li, W. Cai, J. An, S. Kim, J. Nah, D. Yang, R. Piner, A. Velamakanni, I. Jung, E. Tutuc, S.K. Banerjee, L. Colombo, R.S. Ruoff, Large-area synthesis of high-quality and uniform graphene films on copper foils, Science 324 (2009) 1312–1314, https://doi.org/10.1126/science.1171245, 1979.

[9] X. Li, L. Colombo, R.S. Ruoff, Synthesis of graphene films on copper foils by chemical vapor deposition, Adv. Mater. 28 (2016) 6247–6252, https://doi.org/10.1002/adma.201504760.

[10] D.G. Papageorgiou, I.A. Kinloch, R.J. Young, Mechanical properties of graphene and graphene-based nanocomposites, Prog. Mater. Sci. 90 (2017) 75–127, https://doi.org/10.1016/j.pmatsci.2017.07.004.

[11] W. Fu, L. Jiang, E.P. van Geest, L.M.C. Lima, G.F. Schneider, Sensing at the surface of graphene field-effect transistors, Adv. Mater. 29 (2017) 1603610, https://doi.org/10.1002/adma.201603610.

[12] J. Zhan, Z. Lei, Y. Zhang, Non-covalent interactions of graphene surface: mechanisms and applications, Chem 8 (2022) 947–979, https://doi.org/10.1016/j.chempr.2021.12.015.

[13] G. Liu, W. Jin, N. Xu, Two-dimensional-material membranes: a new family of high-performance separation membranes, Angew. Chem. Int. Ed. 55 (2016) 13384–13397, https://doi.org/10.1002/ANIE.201600438.

[14] D. Prasai, J.C. Tuberquia, R.R. Harl, G.K. Jennings, K.I. Bolotin, Graphene: corrosion-inhibiting coating, ACS Nano 6 (2012) 1102–1108, https://doi.org/10.1021/nn203507y.

[15] S. Chen, L. Brown, M. Levendorf, W. Cai, S. Ju, J. Edgeworth, R.S. Ruoff, C.E.T. Al, Oxidation resistance of graphene- coated Cu and Cu /Ni alloy, ACS Nano 5 (2011) 1321–1327, https://doi.org/10.1021/nn103028d.

[16] G. Kalita, M.E. Ayhan, S. Sharma, S.M. Shinde, D. Ghimire, K. Wakita, M. Umeno, M. Tanemura, Low temperature deposited graphene by surface wave plasma CVD as effective oxidation resistive barrier, Corros. Sci. 78 (2014) 183–187, https://doi.org/10.1016/j.corsci.2013.09.013.

[17] Y. Fu, A.V. Rudnev, G.K.H. Wiberg, M. Arenz, Single graphene layer on Pt(111) creates confined electrochemical environment via selective ion transport, Angew. Chem. - Int. Ed. 56 (2017) 12883–12887, https://doi.org/10.1002/anie.201705952.

[18] N. Arulmozhi, S. Hanselman, V. Tudor, X. Chen, D. van Velden, G.F. Schneider, F. Calle-Vallejo, M.T.M. Koper, Energetics and kinetics of hydrogen electrosorption on a graphene-covered Pt(111) electrode, JACS Au 3 (2023) 526–535, https://doi.org/10.1021/jacsau.2c00648.

[19] H. Li, J. Xiao, Q. Fu, X. Bao, Confined catalysis under two-dimensional materials, Proc. Natl. Acad. Sci. U. S. A. 114 (2017) 5930–5934, https://doi.org/10.1073/pnas.1701280114.

[20] Y. Zhou, W. Chen, P. Cui, J. Zeng, Z. Lin, E. Kaxiras, Z. Zhang, Enhancing the hydrogen activation reactivity of nonprecious metal substrates via confined catalysis underneath graphene, Nano Lett. 16 (2016) 6058–6063, https://doi.org/10.1021/acs.nanolett.6b02052.

[21] S. Trasatti, Work function, electronegativity, and electrochemical behaviour of metals. II. Potentials of zero charge and "electrochemical" work functions, J. Electroanal. Chem. 33 (1971) 351–378, https://doi.org/10.1016/S0022-0728(71)80123-7.

[22] J. Clavilier, R. Faure, G. Guinet, R. Durand, Preparation of monocrystalline Pt microelectrodes and electrochemical study of the plane surfaces cut in the direction of the {111} and {110} planes, J. Electroanal. Chem. 107 (1980) 205–209, https://doi.org/10.1016/S0022-0728(79)80022-4.

[23] J. Sun, Y. Nam, N. Lindvall, M.T. Cole, K.B. Kenneth, Y.W. Park, A. Yurgens, Growth mechanism of graphene on platinum: surface catalysis and carbon segregation, Appl. Phys Lett. 104 (2014) 152107, https://doi.org/10.1063/1.4871978/130877.

[24] L. Jin, C. Zhao, Z. Gong, J. Pan, W. Wei, G. Wang, Y. Cui, Hydrogen-promoted graphene growth on Pt(111) via CVD methods, Surf. Interfaces 26 (2021) 101383, https://doi.org/10.1016/j.surfin.2021.101383.

[25] K. Xiao, H. Wu, H. Lv, X. Wu, H. Qian, The study of the effects of cooling conditions on high quality graphene growth by the APCVD method, Nanoscale 5 (2013) 5524–5529, https://doi.org/10.1039/C3NR00524K.

[26] P.H. Ho, Y.T. Liou, C.H. Chuang, S.W. Lin, C.Y. Tseng, D.Y. Wang, C.C. Chen, W. Y. Hung, C.Y. Wen, C.W. Chen, Self-crack-filled graphene films by metallic nanoparticles for high-performance graphene heterojunction solar cells, Adv. Mater. 27 (2015) 1724–1729, https://doi.org/10.1002/adma.201404843.

[27] T. Yoon, J.H. Kim, J.H. Choi, D.Y. Jung, I.J. Park, S.Y. Choi, N.S. Cho, J.I. Lee, Y. D. Kwon, S. Cho, T.S. Kim, Healing graphene defects using selective electrochemical deposition: toward flexible and stretchable devices, ACS Nano 10 (2016) 1539–1545, https://doi.org/10.1021/acsnano.5b07098.

[28] A.J. Shih, N. Arulmozhi, M.T.M. Koper, Electrocatalysis under cover: enhanced hydrogen evolution via defective graphene-covered Pt(111), ACS Catal. 11 (2021) 10892–10901, https://doi.org/10.1021/acscatal.1c02145.

[29] N.M. Markovic, B.N. Grgur, P.N. Ross, Temperature-dependent hydrogen electrochemistry on platinum low-index single-crystal surfaces in acid solutions, J. Phys. Chem. B 101 (1997) 5405–5413, https://doi.org/10.1021/jp970930d.

[30] H.A. Gasteiger, N.M. Markovic, P.N. Ross, H2 and CO electrooxidation on well-characterized Pt, Ru, and Pt-Ru. 1. Rotating disk electrode studies of the pure gases including temperature effects, J. Phys. Chem. 99 (1995) 8290–8301, https://doi.org/10.1021/J100020A063.

[31] J.E. Bao, D.D. Macdonald, Oxidation of hydrogen on oxidized platinum: Part I: the tunneling current, J. Electroanal. Chem. 600 (2007) 205–216, https://doi.org/10.1016/J.JELECHEM.2006.07.024.

[32] H.S. Choo, T. Kinumoto, M. Nose, K. Miyazaki, T. Abe, Z. Ogumi, Electrochemical oxidation of highly oriented pyrolytic graphite during potential cycling in sulfuric acid solution, J. Power Sources 185 (2008) 740–746, https://doi.org/10.1016/j.jpowsour.2008.07.086.

[33] W. Li, M. Wojcik, K. Xu, Optical microscopy unveils rapid, reversible electrochemical oxidation and reduction of graphene, Nano Lett. 19 (2019) 983–989, https://doi.org/10.1021/acs.nanolett.8b04216.

[34] J.A. Quezada-Renteria, C.O. Ania, L.F. Chazaro-Ruiz, J.R. Rangel-Mendez, Influence of protons on reduction degree and defect formation in electrochemically reduced graphene oxide, Carbon 149 (2019) 722–732, https://doi.org/10.1016/j.carbon.2019.04.109.

[35] Z.F. Wu, P.Z. Sun, O.J. Wahab, Y.T. Tan, D. Barry, D. Periyanagounder, P.B. Pillai, Q. Dai, W.Q. Xiong, L.F. Vega, K. Lulla, S.J. Yuan, R.R. Nair, E. Daviddi, P. R. Unwin, A.K. Geim, M. Lozada-Hidalgo, Proton and molecular permeation through the basal plane of monolayer graphene oxide, Nat. Commun. 14 (2023) 7756, https://doi.org/10.1038/s41467-023-43637-w.

[36] L. Gao, W. Ren, H. Xu, L. Jin, Z. Wang, T. Ma, L.P. Ma, Z. Zhang, Q. Fu, L.M. Peng, X. Bao, H.M. Cheng, Repeated growth and bubbling transfer of graphene with millimetre-size single-crystal grains using platinum, Nat. Commun. 3 (2012) 699, https://doi.org/10.1038/ncomms1702.

[37] X. Wang, L. Tao, Y. Hao, Z. Liu, H. Chou, I. Kholmanov, S. Chen, C. Tan, N. Jayant, Q. Yu, D. Akinwande, R.S. Ruoff, Direct delamination of graphene for high-performance plastic electronics, Small 10 (2014) 694–698, https://doi.org/10.1002/smll.201301892.